THE JOURNAL OF PHYSICAL CHEMISTRY A
A JOURNAL OF THE AMERICAN CHEMICAL SOCIETY

pubs.acs.org/JPCA

Article

Photoswitching Molecules Functionalized with Optical Cycling Centers Provide a Novel Platform for Studying Chemical Transformations in Ultracold Molecules

Published as part of The Journal of Physical Chemistry A special issue "Massimo Olivucci Festschrift".

Paweł Wójcik, Taras Khvorost, Guanming Lao, Guo-Zhu Zhu, Antonio Macias, Jr., Justin R. Caram, Wesley C. Campbell, Miguel A. García-Garibay, Eric R. Hudson, Anastassia N. Alexandrova, and Anna I. Krylov*

Cite This: J. Phys. Chem. A 2025, 129, 1929−1940

Read Online

ACCESS | Metrics & More | Article Recommendations | Supporting Information

ABSTRACT: A novel molecular structure that bridges the fields of molecular optical cycling and molecular photoswitching is presented. It is based on a photoswitching molecule azobenzene functionalized with one and two CaO- groups, which can act as optical cycling centers (OCCs). This paper characterizes the electronic structure of the resulting model systems, focusing on three questions: (1) how the electronic states of the photoswitch are impacted by a functionalization with an OCC; (2) how the states of the OCC are impacted by the scaffold of the photoswitch; and (3) whether the OCC can serve as a spectroscopic probe of isomerization. The experimental feasibility of the proposed design and the advantages that organic synthesis can offer in the further functionalization of this molecular scaffold are also discussed. This work brings into the field of molecular optical cycling a new dimension of chemical complexity intrinsic to only polyatomic molecules.

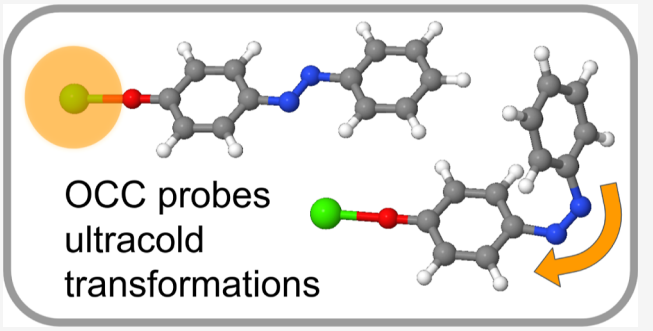

1. INTRODUCTION

The CaO group attached to a molecular scaffold can function as an optical cycling center (OCC). Molecules functionalized with OCCs can be laser cooled by scattering thousands of photons with a minimal loss of the population from the cycling pair of states (preferably the ground state and the lowest excited state). Laser-cooled molecules are exploited in quantum technologies as well as in studies of fundamental physical phenomena[1−16] and ultracold chemistry.[17−29] The idea of using OCCs in polyatomic molecules builds on the success of laser cooling of diatomic molecules.[30−42] The electronic structure of laser-cooled molecules (all the way through hyperfine structure), their applications, and recent experimental advances are thoroughly covered in recent reviews.[43−49]

The CaO- group can function as an OCC because it supplies the molecule with an access to an electronically excited state that spontaneously decays almost exclusively to the molecular (electronic and vibrational) ground state.[50−57] Other quantum functional groups suitable for laser cooling, such as SrO- and YbO-, have also been identified.[57−87]

One—thus far only hypothesized but exciting—possibility is to use quantum functional groups, such as CaO- OCCs, for precise optical sensing of chemical events. For example, it would be desirable to have an optical reporter that can detect a chemical change, such as a conformational change or a chemical reaction, in a part of the molecule distant from the reporter. Because the OCCs are electronically isolated from the rest of the molecule by design, it might appear as a contradiction that an OCC can be used for such a sensing. However, OCCs rely on transitions with narrow line widths, which may feature small but detectable shifts and exhibit other delicate effects such as Fermi resonances arising from accidental degeneracies of vibrational states,[83] all of which may serve as an optical signature of chemical reactions.

As a model reaction to investigate this concept, we have chosen photoisomerization of azobenzene (AB)[88,89] (shown in Figure 1). The photoisomerization of AB from the more stable *trans*-conformation to the less stable *cis*-conformation is triggered by the ultraviolet light of the 300−400 nm wavelength (3.1−4.1 eV),[90,91] which is different from the OCC transition

Received: September 18, 2024
Revised: November 21, 2024
Accepted: November 22, 2024
Published: December 19, 2024

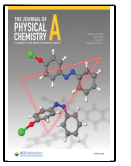

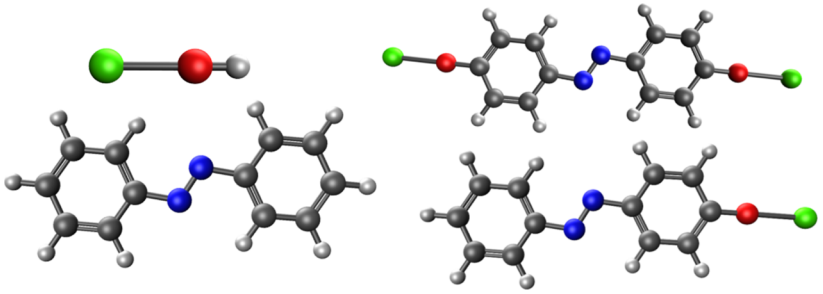

Figure 1. Molecules studied in this work. Counterclockwise from the top left: CaOH, AB, *para*-CaO-AB (pAB), and bis(*para*-CaO)-AB (bpAB).

(about 650 nm or 1.9 eV). Thus, it should be possible to excite the respective transitions independently. In the dark, the *cis*-isomer has a substantial lifetime, slowly relaxing back the *trans*-isomer at room temperature. We hypothesize that an OCC located far from the azo bridge can optically report on photoisomerization—a model chemical event that is relatively easy to probe in the gas phase.

Furthermore, controlling the position and dipole alignment of the OCCs through a chemical or physical handle (such as photoswitching) brings an interesting new dimension into quantum information science (QIS). For this reason, we also study AB decorated with two CaO- OCCs located on each of the two benzene rings. The possibility of chemical sensing with OCCs and controlling the spatial arrangement of multiple OCCs by means of an "orthogonal" chemical transformation is both of fundamental importance and of interest to the field of QIS.

In this contribution, we investigate the electronic structure of molecules comprising the CaO and AB moieties: pAB and bpAB; the relevant structures are shown in Figure 1. The electronic states of pAB are of three types: the electronic states similar to these of the scaffold (AB-like), the electronic states localized on the OCC (OCC-like), and the electronic states of a mixed character.

The quantum-chemical description of such systems is far from trivial, owing to their open-shell character.[52,86,87] We use methods from the equation-of-motion coupled-cluster (EOM-CC) family to describe the relevant electronic states of these molecules. EOM-CC provides a robust and versatile approach to electronically excited and open-shell species.[92−95] As shown in Figure 2, different variants of EOM-CC provide access to different types of states. Molecules with a single unpaired electron (CaOH and pAB) are well described by EOM-EA-CC (EOM-CC for electron attachment). EOM-EE-CC (EOM-CC for excitation energies) describes excited states of closed-shell molecules (AB), but it can also be used for open-shell species, such as pAB. EOM-DEA-CC (EOM-CC for double electron attachment) and EOM-SF-CC (EOM-CC with spin-flipping excitations) are the preferred methods for diradicals (bpAB).[96,97]

The paper is organized as follows. The next section provides details about the computational approach. In section III, we review the electronic structure of the prototype systems (AB and CaOH) and then characterize the electronic states of the pAB and bpAB. We focus on the three questions: (1) How are the states of the scaffold impacted by the OCC? (2) How are the states of the OCC impacted by the scaffold? (3) Can we employ the OCC as a spectroscopic probe of the isomerization reaction? We then discuss preliminary results of the synthetic efforts and outline future directions.

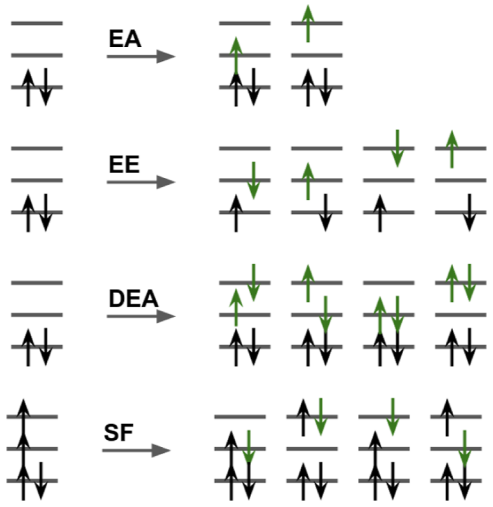

Figure 2. EOM-CC models used in this work. Color illustrates the action of the EOM operator (only single excitations are shown). An EOM method is defined by specifying the reference determinant and the type of generalized excitation operator—e.g., spin and electron-conserving operators are used in EOM-EE, spin-flipping operators are used in EOM-SF, and non particle-conserving operators are used in EOM-EA and EOM-DEA.

2. THEORETICAL METHODS AND COMPUTATIONAL DETAILS

The EOM-CC family of methods[92−95] employs the following ansatz:

$$\Psi = Re^{T}\Phi_0 \tag{1}$$

where Φ_0 is the Hartree−Fock reference determinant and T is the cluster operator

$$T = \sum_{ia} t_i^a a^\dagger i + \frac{1}{2!^2}\sum_{ijab} t_{ij}^{ab} a^\dagger b^\dagger ij + \ldots \tag{2}$$

where the operators $a^\dagger$, $b^\dagger$, i, and j are the fermionic creation and annihilation operators associated with molecular orbitals (MOs) φ_a, φ_b, φ_i, and φ_j. The choice of reference Φ_0 determines the separation between the occupied and virtual spaces.[98] The amplitudes t are found by solving the coupled-cluster equations obtained by projecting the similarity-transformed Schrödinger equation

$$\exp(-T)H\,\exp(T)\Phi_0 = E_{\mathrm{CC}}\Phi_0 \tag{3}$$

onto the space spanned by the reference determinant Φ_0, all singly $\{\Phi_i^a\}$ and doubly $\{\Phi_{ij}^{ab}\}$,... substituted determinants. In this work, we use EOM-CC models with the expansion

https://doi.org/10.1021/acs.jpca.4c06320
J. Phys. Chem. A 2025, 129, 1929−1940

truncated after the second term, EOM-CC with single and double substitutions (EOM-CCSD).

The EOM operator, R, has the form that depends on a particular flavor of EOM (as illustrated in Figure 2). We use EOM-CC methods that are best suited for each type of electronic states studied here:

- EOM-EA-CCSD.[99−101] In this method, the Hartree−Fock reference corresponds to a closed-shell cation and the EOM operator R has one more creation than annihilation operators, giving rise to the EOM-EA-CCSD wave functions of the neutral states. This method is suitable for CaOH and pAB.
- EOM-EE-CCSD.[102] The EOM-EE excitation operator preserves the number of electrons and generates electronically excited states.[93] For the closed-shell references, the excited states are naturally spin adapted, forming singlet or triplet excitations. EOM-EE-CCSD can also be applied to open-shell references, although in this case, the wave functions may be slightly or severely spin contaminated,[92,103,104] depending on the type of an excitation. This method is suitable for AB and pAB, with the caveats discussed below.
- EOM-SF-CCSD.[97,105−108] The EOM-SF operator preserves the number of electrons, but it flips the spin of one electron. This method uses a high-spin (M_s = 1) triplet state as a reference and describes the singlet and the low-spin (M_s = 0) components of the triplet states. The description of the higher-lying states is not accurate due to spin incompleteness.
- EOM-DEA-CCSD.[96,100,109,110] The EOM-DEA operator increases the number of electrons by two. The Hartree−Fock reference for this method is a closed-shell dication. This method is suitable for bpAB; it can describe both diradical states as well as higher excited states, which was exploited in previous studies of molecules with two OCCs (bi-OCCs).[26,86,87]

Below, we provide more details about the computational protocols employed.

2.1. Computational Protocols. We described the electronic states of AB functionalized with a single OCC using the EOM-EA-CCSD method. We also used this method to optimize the structure of the molecule in its ground electronic state. We then used this method to compute the low-lying excited states at the optimized geometry. We note that EOM-EA-CCSD can only accurately describe states dominated by the OCC transitions because states involving MOs of the scaffold will appear as $2p1h$ (two-particle-one-hole) excitations. To gain access to these states, we calculated excited states with the EOM-EE-CCSD starting from an open-shell doublet reference.

We described the AB molecule functionalized with two OCCs with the same methods as in our previous work on bi-OCCs.[26,86,87] We optimized geometry of the ground electronic state with EOM-SF-CCSD[106] and computed the excitation energies at the optimized geometry with the EOM-DEA-CCSD method.

We used Dunning's cc-pVDZ basis set for geometry optimization and aug-cc-pVDZ for excitation energies.[111−113] All CC and EOM-CC calculations were carried out with *Q-Chem*.[114,115] Orbitals and structures were visualized with the *IQmol* and *Jmol* molecular visualization tools.[116,117]

In the Supporting Information, we provide Cartesian coordinates of relevant structures, Franck−Condon factors for the cycling transitions, and results of the calculations with time-dependent density functional theory (TD-DFT).

2.2. Wave Function Analysis. We analyzed transitions between the electronic states using natural transition orbitals (NTOs),[118] which provide the most compact representation of the transition. NTOs are defined as the left and right singular vectors of the one-particle transition density matrix[119−121]

$$\gamma_{pq}^{f\leftarrow i} = \langle \Psi_f | p^\dagger q | \Psi_i \rangle \tag{4}$$

where Ψ_i and Ψ_f are the two states involved in the transition. $\gamma_{pq}^{f\leftarrow i}$ is related to one-particle transition density, $\rho^{f\leftarrow i}(r_h, r_p)$

$$\begin{aligned}\rho^{f\leftarrow i}(r_h, r_p) &= N \int \Psi_i(r_h, r_2, ..., r_n)\Psi_f(r_p, r_2, ..., r_n)\mathrm{d}r_2 ... \mathrm{d}r_n \\ &= \sum_{pq} \gamma_{pq}^{f\leftarrow i} \varphi_p(r_p)\varphi_q(r_h),\end{aligned} \tag{5}$$

where N is the number of electrons.

Visual inspection of the NTOs enables the characterization of the electronic states. However insightful, such analysis can be tedious and somewhat subjective. The wave function analysis tools afford direct extraction of information about the character of the wave function. We use the *TheoDORE* package to automate this analysis.[122] In particular, we are interested in the extent of charge transfer between the scaffold and the OCCs, which can be used to quantify the extent of electronic coupling between the two moieties. Charge-transfer numbers (CTNs) are exciton descriptors, which provide a measure of charge transfer between different parts of the system. The partition of electrons between fragments A and B is given by integrating the $\gamma^{f\leftarrow i}$ over restricted regions

$$\Omega_{AB} = \int_A \mathrm{d}r_h \int_B \mathrm{d}r_p \left|\gamma(r_h, r_p)\right|^2 \tag{6}$$

Thus, CTNs can be interpreted as the number of electrons transferred between A and B. In these calculations, the only user-required input is a partition of the molecule into fragments.[122] This analysis depends on the definition of the region boundaries, similar to the Mulliken charges.

3. RESULTS AND DISCUSSION

3.1. Electronic Structure of AB and CaOH. We begin by reviewing the electronic states of AB and CaOH. Figure 3 shows relevant MOs.

The ground state AB is a closed-shell singlet. The excited states of AB are derived by promotion of an electron from the nitrogen (azo) bridge—relevant MOs are π and lone-pair n (see Figure 3). The first excited singlet state is a dark $n\pi^*$ transition. The second excited singlet state is a bright $\pi\pi^*$ transition. At the EOM-EE-CCSD/aug-cc-pVDZ level of theory, the energies of these transitions are 3.055 and 4.465 eV, respectively. In both states, electrons of the nitrogen bridge MOs are promoted to an antibonding orbital, effectively weakening the double bond and lowering the barrier along the *cis*−*trans* rotation coordinate. Below, we refer to the excited states generated by transitions localized on the AB scaffold as the AB-like states or the scaffold-like states.

Next, we review the electronic states of CaOH, which can be described as a hydrogen-terminated OCC. Extensive spectroscopic data is available for this molecule.[123−130] CaOH is one of a few polyatomic molecules that have been laser cooled, paving the way for advanced quantum-state control experiments.[131−137] CaOH is a doublet radical with one unpaired electron localized

https://doi.org/10.1021/acs.jpca.4c06320
J. Phys. Chem. A 2025, 129, 1929−1940

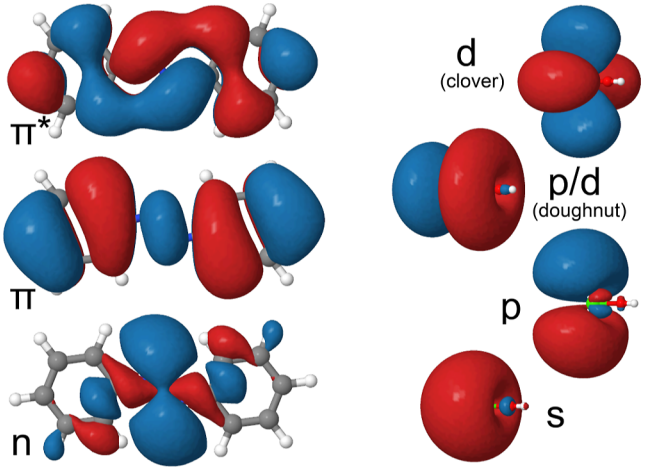

Figure 3. NTOs of the relevant electronic transitions in the *trans*-AB (left) and CaOH (right).

on the metal. The low-lying electronic states of CaOH resemble the states of an alkali atom (Figure 3). Both ground and the low-lying excited electronic states can be described as a closed-shell core with a single valence electron occupying hydrogen-atom-like orbitals. In the ground state (X state), the unpaired electron is localized on the Ca atom, resembling the ^{2}S atomic state. The first pair of excited states (A and B states) are ^{2}P-like states, with degeneracy lifted in nonlinear structures. The X → A transition energy for CaOH is around 2 eV. Higher CaOH states also follow this pattern of a localized atomic-like transition of a single unpaired electron. Below, we refer to these states as OCC-like states. This type of states is commonly found in molecules functionalized with the CaO- group.[57,79,131,138]

3.2. Electronic States of pAB. The electronic states of pAB can be classified as either AB-like, OCC-like, or states of mixed character. The key question is the extent to which the AB-like and the OCC-like states perturb each other. Previously, the effect of the electronic states of the scaffold on the OCC-like states was explored by Dickerson and co-workers.[77,78] They found that when the energy of the first excited state in the unfunctionalized scaffold comes close to the energy of the cycling transition, the two electronic states begin to interact, spoiling the localized character of the OCC transitions. Here, we apply a similar analysis to electronic states of functionalized AB.

We begin exploring an interplay between the OCC and AB moieties by inspecting the electronic states of a singly functionalized molecule, pAB, in which the CaO- group is located at the para position with respect to the nitrogen bridge (see Figure 1). Placing the CaO- group in the *para* position minimizes the steric repulsion, which is favorable for laser cooling.[79]

The electronic states of pAB, the molecule comprising CaOH and AB moieties, can be correlated to the states of its building blocks. Similar to other molecules functionalized with CaO- groups, the low-lying states of *trans*-pAB are clearly identifiable as OCC like. The first state with non-OCC features appears at 3.5 eV as the sixth excited doublet state. This state derives from a π^* orbital on the azo bridge with a p/d admixture on the metal. The transition to this state differs from the S_0 to S_1 transition of *trans*-AB as it does not originate from a promotion of a lone-pair n to the π^* orbital; rather, it is the s-type orbital of the OCC which is excited. Interestingly, the next two states recover the OCC-like character and can be identified as s-like and p/d-like.

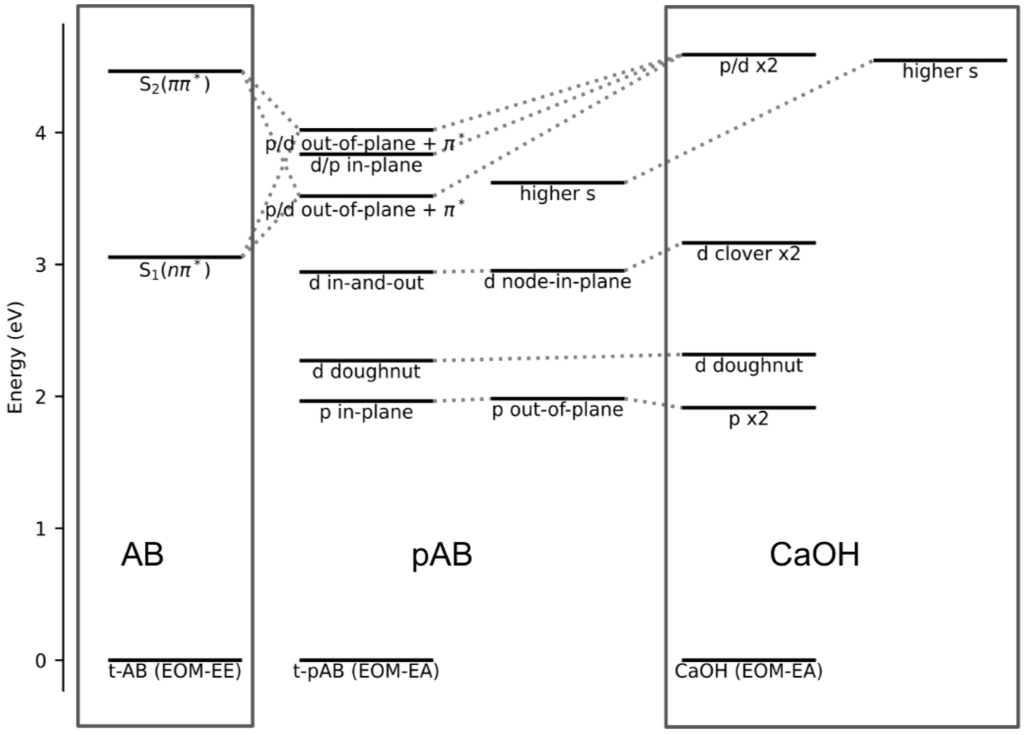

Figure 4. Electronic states of *trans*-pAB (central panel; EOM-EA-CCSD/aug-cc-pVDZ at the EOM-EA-CCSD/cc-pVDZ geometry) as a combination of *trans*-AB states (the column on the left; EOM-EE-CCSD/aug-cc-pVDZ at the CCSD/cc-pVDZ geometry) and the OCC states (CaOH; two columns on the right; EOM-EA-CCSD/aug-cc-pVDZ at the EOM-EA-CCSD/cc-pVDZ geometry). Energies of the respective ground states are set to zero.

https://doi.org/10.1021/acs.jpca.4c06320
J. Phys. Chem. A 2025, 129, 1929−1940

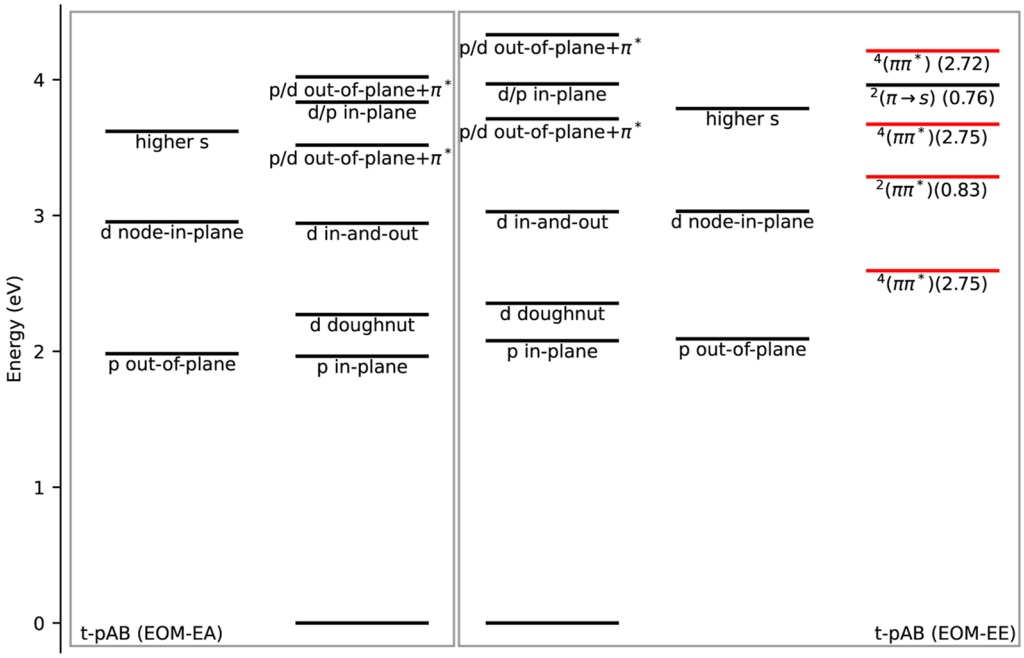

Figure 5. *Trans*-pAB at the EOM-EA-CCSD/cc-pVDZ geometry. Comparison of the EOM-EA-CCSD/aug-cc-pVDZ states (two columns on the left) with the states computed with EOM-EE-CCSD/aug-cc-pVDZ (three columns on the right). The rightmost column shows the EOM-EE-CCSD states absent in the EOM-EA-CCSD calculations; some of these extra states are spin contaminated (red color); the corresponding values of $\langle S^2 \rangle$ are given in the parentheses.

The ninth excited state located vertically at 4.0 eV is of a mixed character.

Figure 4 summarizes the electronic states of *trans*-pAB. The states of an OCC-like character are preserved for excitation energies below the first excited state of the unfunctionalized AB, but some of the OCC-like states are also present above this threshold. The states of mixed character appear close to and above this threshold.

As explained in the methods section, different flavors of EOM-CCSD are suitable for different types of states. In the case of pAB, we expect that EOM-EA-CCSD describes well the transitions localized on the OCC, but it yields less accurate results for the transitions involving the scaffold orbitals. To gain a better handle on these states, we employ EOM-EE-CCSD. We also present wave function analysis of the resulting states.

The method of choice for the treatment of the excited states of AB is EOM-EE; however, using this method for the pAB molecule is complicated by its open-shell character, which can lead to small or severe spin contamination.[92,103,104] Generally, states derived by excitations to or from open-shell orbitals are well behaved,[92] whereas the states derived by excitations from doubly occupied to unoccupied orbitals are poorly described because of the spin incompleteness of the EOM-EE-CCSD ansatz (this problem can be remedied by including selected triple excitations[139]).

In *trans*-pAB, the spin contamination of the reference Hartree−Fock determinant is small; it is also rather small for the most low-lying EOM states (∼0.002). The EOM-EE-CCSD method yields the spectrum of *trans*-pAB that qualitatively agrees with the EOM-EA-CCSD one. The EOM-EE-CCSD excitation energies are higher by about 0.15 eV. The transition dipole moments are within 30% of the EOM-EA-CCSD values.

The EOM-EE-CCSD calculations also yield a set of states that do not have counterparts among the EOM-EA-CCSD states. As anticipated, the EOM-EE-CCSD method yields excited states derived by promoting electrons localized on the AB moiety. These states can be classified as AB-like states of the $\pi \rightarrow \pi^*$ type. One of the new states should again be characterized as a state of mixed character, as it derives from the $\pi \rightarrow s$(Ca) transition. Some of the AB-like states (especially quartets) show high spin-contamination, which indicates that their proper description would require inclusion of higher terms in the EOM-CC expansion (see Figure 25 and the corresponding discussion in ref 92). Figure 5 highlights the differences between the EOM-EA-CCSD and EOM-EE-CCSD results.

Having described this manifold of excited states, we conclude this section by presenting the CTN-based analysis of their corresponding wave functions (pAB is partitioned into CaO- and the rest). Here, CTNs can be interpreted as the number of electrons transferred between the OCC and AB moieties—perfectly isolated localized transitions can be identified by zero CTNs. Figure 6 shows the CTNs and state energies. We highlight the following observations:

- Among states classified as OCC-like, the transitions are indeed localized on the CaO- moiety.
- The main outlier is the state visually assigned as *d* (doughnut). Figure 7 shows NTOs for that state. Although, visually, the state appears to be localized on the CaO- group, the CTN analysis shows that a significant portion of the electronic density is ascribed to the AB fragment. A similar observation about the analogous $B^2\Sigma^+$ state of SrOH was made in the previous study, where a significant contribution to the state was attributed to hydrogen's *s* orbital.[53]
- The sum of all CTNs gives the norm of the one particle transition density, $\|\gamma\|$. The difference, $1 - \|\gamma\|$, quantifies the multiply excited character of the state. Spin-contaminated states are all ranking the highest in this metric, confirming that higher excited configurations are needed for a proper description of these states.

https://doi.org/10.1021/acs.jpca.4c06320
J. Phys. Chem. A 2025, 129, 1929−1940

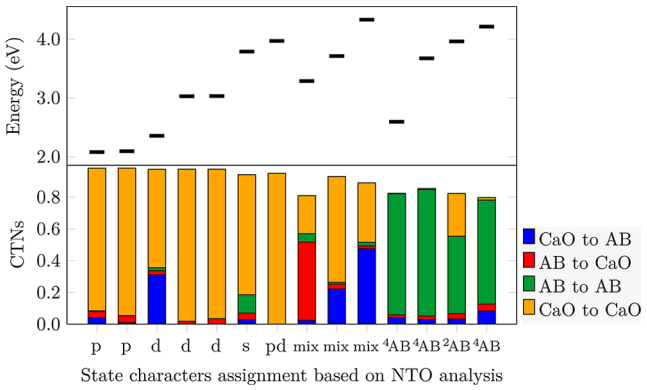

Figure 6. Electronic states of *trans*-pAB and the character of the underlying wave functions. Top: state energies (relative to the ground state). Bottom: CTNs characterizing the transitions from the ground state. The states are ordered from left to right to match three groups: first are the OCC-like states (labeled *s*, *p*, and *d*), second are the states of a mixed character (mix), and the last are the AB-like states (labeled $^{2S+1}$AB). Compare with Figure 5. EOM-EE-CCSD/aug-cc-pVDZ at the EOM-EA-CCSD/cc-pVDZ ground state geometry.

- CTNs highlight that the states labeled as of a mixed character are formed by promoting the ground state *s*(Ca) electron to an orbital delocalized over the CaO- and AB moieties, or the other way around.

3.3. OCC as a Spectroscopic Probe to Monitor Isomerization. The key feature of AB, which carries over to its functionalized versions, is its ability to assume two distinct geometries, namely, the *cis*- and *trans*-isomers. Well known in photochemistry, this is a new element in the context of molecules functionalized with OCCs.

The different structures of the two isomers of pAB make the two systems distinct, just as if the OCCs were attached to two different scaffolds. The impact of the scaffold on the properties of an OCC, which is of a central importance in the context of laser cooling, has been extensively studied.[26,52,55,57,71,76−82,86,87] Yet, the effect of the scaffold isomerization on the OCC states has not been investigated. Furthermore, what makes pAB special is that *cis*- and *trans*-isomers can be interconverted. Such chemical complexity, unique to polyatomic molecules, can be a useful resource to QIS applications.

We now consider the other isomer of pAB, *cis*-pAB, and compare the low-lying excited states of the two isomers using the same computational protocol as above. The low-lying electronic states of *cis*-pAB are identified as OCC-like. Table 1 highlights similarities in the X → A and X → B transitions in *trans*-pAB, *cis*-pAB, and CaOH.

The key result of this calculation is the impact of the isomerization on the excitation energy of the cycling transition, X → A. Although this value can be affected by a change in the ligand, the computed excitation energy change due to the isomerization is minute (on the order of 1 meV). Thus, pAB results show that AB acts, to a large extent, as an inert scaffold, carrying the OCC in space without affecting the characteristics of the cycling transition. This can be rationalized by the observation that in the gas phase, the OCC does not experience large variations in its environment between the *trans*- and *cis*-isomers. Hence, one can imagine a scenario in which the inert AB scaffold can move the OCC to a different local environment.

Table 1. Excitation Energies (in eV) and Oscillator Strengths (in Parentheses) of the *trans*-pAB, *cis*-pAB, and CaOH Calculated with EOM-EA-CCSD/aug-cc-pVDZ at the EOM-EA-CCSD/cc-pVDZ Geometries[a]

transition	*trans*-pAB	*cis*-pAB	CaOH
X → A	1.964 (0.262)	1.964 (0.260)	1.915 (0.291)
X → B	1.983 (0.272)	1.980 (0.268)	1.915 (0.291)

[a]EOM convergence threshold 10^{-10}.

To create a situation when the environment of an OCC changes more drastically upon isomerization, we consider the AB scaffold with both phenyl rings functionalized in the *para* position with the CaO- moieties (bpAB), as shown in Figure 8.

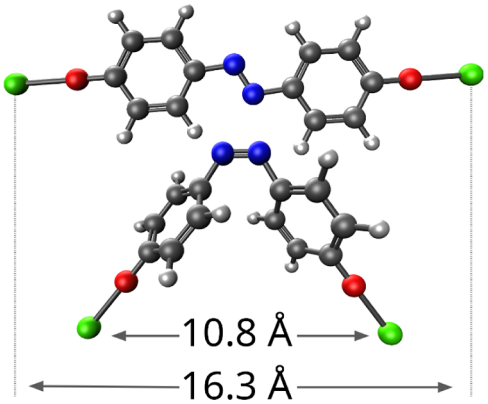

Figure 8. AB molecule functionalized with two OCCs, bpAB. The isomerization reduces the distance between the two Ca atoms from 16.3 to 10.8 Å. Geometries optimized with EOM-SF-CCSD/cc-pVDZ.

In contrast to the isomerization of pAB, where the CaO- group did not sense large changes to its chemical environment, the isomerization of bpAB changes the distance between the two polar CaO- groups.

The optimized geometries of the two isomers show that the structure of the CaO moieties is preserved, meaning that the interactions between the two OCCs are weak and do not induce changes in the overall bonding pattern. The excitation energy from the ground state to the first exited state is shifted; this is an expected outcome related to the change in the electron-withdrawing strength of the ligand.

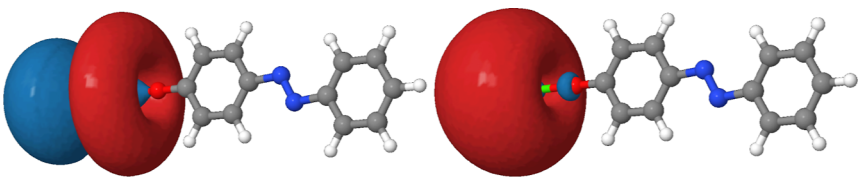

Figure 7. Particle and hole NTOs for the *d*(Ca) (doughnut) state of *trans*-pAB. EOM-EE-CCSD/aug-cc-pVDZ at the EOM-EA-CCSD/cc-pVDZ geometry of the ground state.

https://doi.org/10.1021/acs.jpca.4c06320
J. Phys. Chem. A 2025, 129, 1929−1940

The *trans*-to-*cis* isomerization reduces the distance between the two Ca atoms by almost one-third of its initial value (see Figure 8). Thus, we expect to observe a response to the isomerization in the OCC's optical properties. Table 2 shows the changes in the excitation energy upon isomerization. In contrast to pAB, bpAB shows a much more appreciable change in the excitation energy.

Table 2. Changes in Excitation Energy (eV) for the X → A and X → B Transitions upon Isomerization in Bare pAB and bpAB with an Interacting Group at Both Ends; EOM-EA-CCSD/aug-cc-pVDZ (pAB) and EOM-DEA-CCSD/aug-cc-pVDZ (bpAB)[a,b]

	pAB (X → A)	bpAB (X → A)	pAB (X → B)	bpAB (X → B)
cis	1.964	1.968	1.980	2.002
trans	1.964	2.000	1.983	2.006
change	≲0.001	0.032	0.003	0.004

[a]Using geometries optimized as described in the methods section. [b]EOM convergence threshold 10^{-10}.

We also computed the excitation energies for the second transition (X → B). The changes are smaller than for the X → A transition, likely because the out-of-plane orbitals are aligned at an angle relative to the aromatic rings, which impacts the through-space interaction (see Figure S1 in the Supporting Information).

3.4. Synthetic Efforts: Preliminary Results and Future Work. CaO-AB can be produced by reacting the precursor ligand 4-hydroxyazobenzene (*trans* form purchased from Sigma-Aldrich) with metastable Ca atoms generated by laser ablation in a cryogenic buffer gas cell, as previously discussed in the context of the production of $CaOC_6H_4$ molecules and their functionalized derivatives.[57,80,83] However, initial experiments have revealed that the yellow powder of 4-hydroxyazobenzene undergoes a color change to black at ∼100 °C, well below its melting point of 155 °C. This suggests the thermal decomposition of AB,[140] making it unlikely to generate sufficient precursor vapors for the reaction. To address this issue, the precursor can be functionalized with electron-withdrawing groups, such as fluorine atoms, to enhance its thermal stability.[140] Alternatively, a solid-phase method[79] can be adopted. A mixture of CaH_2 and precursor powder (1:1 molar ratio), with poly(ethylene glycol) or silver powder as a binder, can be thoroughly mixed and ground before being pressed into a pellet for direct laser ablation. Preliminary results with the Sr equivalent have shown two peaks in the excitation spectra. Further experiments using CaH_2 and the precursor to produce CaO-AB will be performed. In addition, the precursor ligand exists only in the *trans*-isomeric form, enabling photoswitching to the *cis* isomer upon laser illumination. Specifically, the precursor 4-hydroxybenzene has been reported to undergo photoswitching at ∼360 nm (3.44 eV).[90,91] A 360 nm UV LED or pulsed Nd/YAG laser at 355 nm (3.49 eV) can be employed to initiate the photoswitching of CaO-AB. To measure the branching ratios of the X → A and X → B transitions of these molecules, dispersed laser-induced fluorescence spectroscopy can be taken either with a pulsed dye laser used in the previous works[80,83] or with a continuous-wave (CW) dye laser which is being installed in our lab. The narrow line width and the broad scanning range of the CW dye laser allow us to significantly suppress the background noise, enabling us to obtain high-resolution spectra of these AB molecules.

With many AB derivatives commercially available, the properties of the OCC-photoswitch system can be tuned using varying functionalizations. Several synthetic routes can access derivatives that are not commercially available. A widely used synthetic route involves diazotizing an aromatic amine using sodium nitrite in the presence of strong acid to afford the resulting diazonium salt, which can then be coupled with phenol to give the AB product (Figure 9a).[141,142] Alternatively, the Mills reaction can also be used, where an aromatic amine is oxidized to a nitroso intermediate (Figure 9a). This species can then be reacted with a separate aromatic amine to yield the AB. For symmetric ABs (bi-OCCs), the desired product can be afforded through reductive coupling of aromatic nitro compounds using a reducing agent or oxidative coupling of aromatic amines using an oxidizing agent to achieve the same transformation (Figure 9b).[141,142]

4. CONCLUSIONS AND OUTLOOK

We have presented a comprehensive study of electronically excited states in a model photoswitch molecule functionalized with one or two OCCs. Using state-of-the art *ab initio* methods, the calculations reveal that some states of the functionalized AB preserve their original character, while other states acquire mixed character. The excited-state analysis shows how the atomic-like and scaffold-like character becomes mixed at excitation energies close to and above the first excitation energy of the unfunctionalized scaffold. We have characterized the new type of states that arise from the mixing. The complete description of these states is challenging, and the use of higher-order CC methods may be necessary not only to achieve high accuracy but also for qualitative agreement. Interestingly,

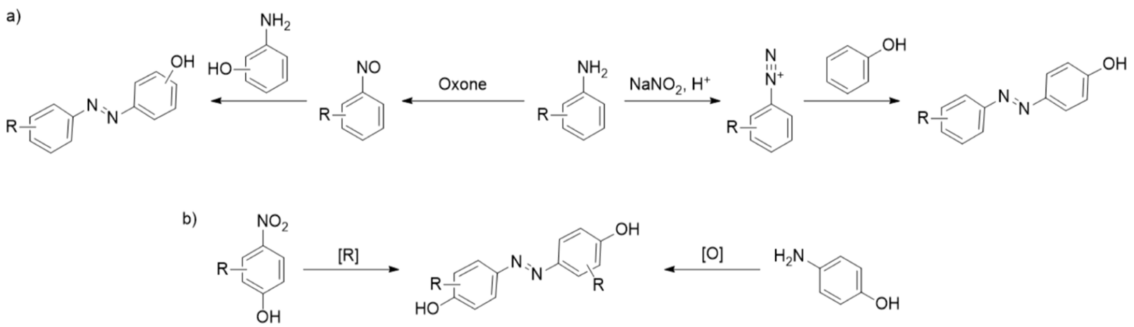

Figure 9. (a) Synthetic routes for asymmetric AB derivatives using Mills reaction (left) and diazotization method (right). (b) Synthetic routes for symmetric AB derivatives.

https://doi.org/10.1021/acs.jpca.4c06320
J. Phys. Chem. A 2025, 129, 1929−1940

we have found OCC-like states even at energies above the energy of the first excited state of the scaffold.

Following the extensive characterization of the relevant electronic states, we have considered spectroscopic signatures of the scaffold's isomerization. The calculations show that the OCC can witness and report on the isomerization process. The AB's scaffold affects the excitation energy of the OCCs thus allowing it to report on its changing environment. Functionalization of the AB's frame with a second OCC results in a model system in which the first OCC can detect anisotropy of the space through which the isomerization reaction takes it. Probing this process via OCCs differs from traditional UV−vis transient absorption, as one can use lower excitation energies and follow much narrower transitions. Furthermore, UV−vis measurements are typically probing ensembles of molecules. OCCs capable of cycling about 100 photons allow for such measurement to be performed on individual, trapped, ultracold molecules. The measurement requires only access to the lowest excited states and assures little to no changes in the final states of the molecules. Thus, in the regime when the experiment targets an individual, trapped, ultracold molecule, OCC probes offer a great advantage.

The presented model system of OCCs attached to organic scaffolds opens up several venues for future research. Possibilities for modifications of the organic scaffold are as rich as the chemistry of photoswitches. In particular, one may explore the stability of the system, the range of structural changes induced by the isomerization or fine-tuning of the transition properties. The latter can also be studied by considering different (or multiple) metals in the various types of OCCs. In this work, we did not discuss the mechanism of the isomerization; rather, we focused on exploring the idea of using OCCs as optical reporters. The results indicate that the use of OCCs can indeed be employed to probe chemical transformations, in particular, for studying ultracold, trapped molecules. One can even imagine the photoswitch considered in this work as a building block for producing larger, multiswitch systems, where the distance and interactions between many OCCs are manipulated by structural realignments.

■ ASSOCIATED CONTENT

Data Availability Statement

The data that support the findings of this study are available within the article and the associated Supporting Information.

Supporting Information

The Supporting Information is available free of charge at https://pubs.acs.org/doi/10.1021/acs.jpca.4c06320.

DFT benchmarks; NTOs for X → B transition; Franck−Condon factors; and Cartesian coordinates of relevant structures (PDF)

■ AUTHOR INFORMATION

Corresponding Author

Anna I. Krylov − *Department of Chemistry, University of Southern California, Los Angeles, California 90089, United States;* orcid.org/0000-0001-6788-5016; Email: krylov@usc.edu

Authors

Paweł Wójcik − *Department of Chemistry, University of Southern California, Los Angeles, California 90089, United States;* orcid.org/0000-0002-8403-9097

Taras Khvorost − *Department of Chemistry and Biochemistry, University of California, Los Angeles, California 90095, United States;* orcid.org/0009-0005-3752-024X

Guanming Lao − *Department of Physics and Astronomy, University of California, Los Angeles, California 90095, United States*

Guo-Zhu Zhu − *Department of Physics and Astronomy, University of California, Los Angeles, California 90095, United States;* orcid.org/0000-0002-5635-3679

Antonio Macias, Jr. − *Department of Chemistry and Biochemistry, University of California, Los Angeles, California 90095, United States*

Justin R. Caram − *Department of Chemistry and Biochemistry, University of California, Los Angeles, California 90095, United States; Center for Quantum Science and Engineering, University of California, Los Angeles, California 90095, United States;* orcid.org/0000-0001-5126-3829

Wesley C. Campbell − *Department of Physics and Astronomy, Center for Quantum Science and Engineering, and Challenge Institute for Quantum Computation, University of California, Los Angeles, California 90095, United States*

Miguel A. García-Garibay − *Department of Chemistry and Biochemistry, University of California, Los Angeles, California 90095, United States;* orcid.org/0000-0002-6268-1943

Eric R. Hudson − *Department of Physics and Astronomy, Center for Quantum Science and Engineering, and Challenge Institute for Quantum Computation, University of California, Los Angeles, California 90095, United States*

Anastassia N. Alexandrova − *Department of Chemistry and Biochemistry, University of California, Los Angeles, California 90095, United States; Center for Quantum Science and Engineering, University of California, Los Angeles, California 90095, United States;* orcid.org/0000-0002-3003-1911

Complete contact information is available at: https://pubs.acs.org/10.1021/acs.jpca.4c06320

Notes

The authors declare the following competing financial interest(s): A.I.K. is the president and a part-owner of Q-Chem, Inc.

■ ACKNOWLEDGMENTS

This work was funded by the NSF Center for Chemical Innovation Phase I (grant no. CHE-2221453).

■ REFERENCES

(1) Kozyryev, I.; Hutzler, N. R. Precision measurement of time-reversal symmetry violation with laser-cooled polyatomic molecules. *Phys. Rev. Lett.* **2017**, *119*, 133002.

(2) Acín, A.; Bloch, I.; Buhrman, H.; Calarco, T.; Eichler, C.; Eisert, J.; Esteve, D.; Gisin, N.; Glaser, S. J.; Jelezko, F.; et al. The quantum technologies roadmap: a European community view. *New J. Phys.* **2018**, *20*, 080201.

(3) Safronova, M. S.; Budker, D.; DeMille, D.; Kimball, D. F. J.; Derevianko, A.; Clark, C. W. Search for new physics with atoms and molecules. *Rev. Mod. Phys.* **2018**, *90*, 025008.

(4) Blackmore, J. A.; Caldwell, L.; Gregory, P. D.; Bridge, E. M.; Sawant, R.; Aldegunde, J.; Mur-Petit, J.; Jaksch, D.; Hutson, J. M.; Sauer, B. E.; Tarbutt, M. R.; Cornish, S. L. Ultracold molecules for quantum simulation: rotational coherences in CaF and RbCs. *Quantum Sci. Technol.* **2019**, *4*, 014010.

(5) Albert, V. V.; Covey, J. P.; Preskill, J. Robust encoding of a qubit in a molecule. *Phys. Rev. X* **2020**, *10*, 031050.

(6) Hutzler, N. R. Polyatomic molecules as quantum sensors for fundamental physics. *Quantum Sci. Technol.* **2020**, *5*, 044011.
(7) Kozyryev, I.; Lasner, Z.; Doyle, J. M. Enhanced sensitivity to ultralight bosonic dark matter in the spectra of the linear radical SrOH. *Phys. Rev. A* **2021**, *103*, 043313.
(8) Fitch, N. J.; Lim, J.; Hinds, E. A.; Sauer, B. E.; Tarbutt, M. R. Methods for measuring the electron's electric dipole moment using ultracold YbF molecules. *Quantum Sci. Technol.* **2021**, *6*, 014006.
(9) Gaul, K.; Berger, R. Global analysis of CP-violation in atoms, molecules and role of medium-heavy systems. *J. High Energy Phys.* **2024**, *2024*, 100.
(10) Arrowsmith-Kron, G.; Athanasakis-Kaklamanakis, M.; Au, M.; Ballof, J.; Berger, R.; Borschevsky, A.; Breier, A. A.; Buchinger, F.; Budker, D.; Caldwell, L.; Charles, C.; Dattani, N.; De Groote, R. P.; DeMille, D.; Dickel, T.; Dobaczewski, J.; Düllmann, C. E.; Eliav, E.; Engel, J.; Fan, M.; Flambaum, V.; Flanagan, K. T.; Gaiser, A. N.; Garcia Ruiz, R. F.; Gaul, K.; Giesen, T. F.; Ginges, J. S. M.; Gottberg, A.; Gwinner, G.; Heinke, R.; Hoekstra, S.; Holt, J. D.; Hutzler, N. R.; Jayich, A.; Karthein, J.; Leach, K. G.; Madison, K. W.; Malbrunot-Ettenauer, S.; Miyagi, T.; Moore, I. D.; Moroch, S.; Navratil, P.; Nazarewicz, W.; Neyens, G.; Norrgard, E. B.; Nusgart, N.; Pašteka, L. F.; N Petrov, A.; Plaß, W. R.; Ready, R. A.; Pascal Reiter, M.; Reponen, M.; Rothe, S.; Safronova, M. S.; Scheidenberger, C.; Shindler, A.; Singh, J. T.; Skripnikov, L. V.; Titov, A. V.; Udrescu, S.-M.; Wilkins, S. G.; Yang, X. Opportunities for fundamental physics research with radioactive molecules. *Rep. Prog. Phys.* **2024**, *87*, 084301.
(11) Ho, C. J.; Lim, J.; Sauer, B. E.; Tarbutt, M. R. Measuring the nuclear magnetic quadrupole moment in heavy polar molecules. *Front. Phys.* **2023**, *11*, 1086980.
(12) Jain, S. P.; Hudson, E. R.; Campbell, W. C.; Albert, V. V. Æ codes. *arXiv* **2023**, 2311.12324. arXiv preprint
(13) Cornish, S. L.; Tarbutt, M. R.; Hazzard, K. R. A. Quantum computation and quantum simulation with ultracold molecules. *Nat. Phys.* **2024**, *20*, 730.
(14) Albert, V. V.; Kubischta, E.; Lemeshko, M.; Liu, L. R. Topology and entanglement of molecular phase space. *arXiv* **2024**, 2403.04572. arXiv preprint
(15) Mitra, D.; Leung, K. H.; Zelevinsky, T. Quantum control of molecules for fundamental physics. *Phys. Rev. A* **2022**, *105*, 040101.
(16) DeMille, D.; Hutzler, N. R.; Rey, A. M.; Zelevinsky, T. Quantum sensing and metrology for fundamental physics with molecules. *Nat. Phys.* **2024**, *20*, 741.
(17) Carr, L. D.; DeMille, D.; Krems, R. V.; Ye, J. Cold and ultracold molecules: science, technology and applications. *New J. Phys.* **2009**, *11*, 055049.
(18) Bell, M. T.; Softley, T. P. Ultracold molecules and ultracold chemistry. *Mol. Phys.* **2009**, *107* (2), 99.
(19) Bohn, J. L.; Rey, A. M.; Ye, J. Cold molecules: Progress in quantum engineering of chemistry and quantum matter. *Science* **2017**, *357*, 1002.
(20) Hutson, J. M. Ultracold chemistry. *Science* **2010**, *327*, 788.
(21) Ospelkaus, S.; Ni, K.-K.; Wang, D.; De Miranda, M. H. G.; Neyenhuis, B.; Quéméner, G.; Julienne, P. S.; Bohn, J. L.; Jin, D. S.; Ye, J. Quantum-state controlled chemical reactions of ultracold potassium-rubidium molecules. *Science* **2010**, *327*, 853.
(22) Dulieu, O.; Krems, R.; Weidemüller, M.; Willitsch, S. Physics and chemistry of cold molecules. *Phys. Chem. Chem. Phys.* **2011**, *13*, 18703.
(23) Quemener, G.; Julienne, P. S. Ultracold molecules under control. *Chem. Rev.* **2012**, *112*, 4949.
(24) Balakrishnan, N. Perspective: Ultracold molecules and the dawn of cold controlled chemistry. *J. Chem. Phys.* **2016**, *145*, 150901.
(25) Wójcik, P.; Korona, T.; Tomza, M. Interactions of benzene, naphthalene, and azulene with alkali-metal and alkaline-earth-metal atoms for ultracold studies. *J. Chem. Phys.* **2019**, *150*, 234106.
(26) Ivanov, M. V.; Bangerter, F. H.; Wójcik, P.; Krylov, A. I. Towards ultracold organic chemistry: Prospects of laser cooling large organic molecules. *J. Phys. Chem. Lett.* **2020**, *11*, 6670.
(27) Bohn, J. L.; Lewandowski, H. J. Cold Chemistry. *J. Phys. Chem. A* **2023**, *127*, 7869.
(28) Luke, J.; Zhu, L.; Liu, Y. X.; Ni, K. K. Reaction interferometry with ultracold molecules. *Faraday Discuss.* **2024**, *251*, 63−75.
(29) Cornish, S. L.; Tarbutt, M. R.; Hazzard, K. R. A. Quantum computation and quantum simulation with ultracold molecules. *Nat. Phys.* **2024**, *20*, 730−740.
(30) Rosa, M. D. Laser-cooling molecules. *Eur. Phys. J. D* **2004**, *31*, 395−402.
(31) Shuman, E. S.; Barry, J. F.; DeMille, D. Laser cooling of a diatomic molecule. *Nature* **2010**, *467*, 820.
(32) Hummon, M. T.; Yeo, M.; Stuhl, B. K.; Collopy, A. L.; Xia, Y.; Ye, J. 2D magneto-optical trapping of diatomic molecules. *Phys. Rev. Lett.* **2013**, *110*, 143001.
(33) Zhelyazkova, V.; Cournol, A.; Wall, T. E.; Matsushima, A.; Hudson, J. J.; Hinds, E. A.; Tarbutt, M. R.; Sauer, B. E. Laser cooling and slowing of CaF molecules. *Phys. Rev. A* **2014**, *89*, 053416.
(34) Norrgard, E. B.; Edwards, E. R.; McCarron, D. J.; Steinecker, M. H.; DeMille, D.; Alam, S. S.; Peck, S. K.; Wadia, N. S.; Hunter, L. R. Hyperfine structure of the $B^3\Pi_1$ state and predictions of optical cycling behavior in the $X \rightarrow B$ transition of TlF. *Phys. Rev. A* **2017**, *95*, 062506.
(35) Lim, J.; Almond, J. R.; Trigatzis, M. A.; Devlin, J. A.; Fitch, N. J.; Sauer, B. E.; Tarbutt, M. R.; Hinds, E. A. Laser cooled YbF molecules for measuring the electron's electric dipole moment. *Phys. Rev. Lett.* **2018**, *120*, 123201.
(36) McNally, R. L.; Kozyryev, I.; Vazquez-Carson, S.; Wenz, K.; Wang, T.; Zelevinsky, T. Optical cycling, radiative deflection and laser cooling of barium monohydride ($^{138}Ba^1H$). *New J. Phys.* **2020**, *22*, 083047.
(37) Albrecht, R.; Scharwaechter, M.; Sixt, T.; Hofer, L.; Langen, T. Buffer-gas cooling, high-resolution spectroscopy, and optical cycling of barium monofluoride molecules. *Phys. Rev. A* **2020**, *101*, 013413.
(38) Zhang, Y.; Zeng, Z.; Liang, Q.; Bu, W.; Yan, B. Doppler cooling of buffer-gas-cooled barium monofluoride molecules. *Phys. Rev. A* **2022**, *105*, 033307.
(39) Vázquez-Carson, S. F.; Sun, Q.; Dai, J.; Mitra, D.; Zelevinsky, T. Direct laser cooling of calcium monohydride molecules. *New J. Phys.* **2022**, *24*, 083006.
(40) Daniel, J. R.; Shaw, J. C.; Wang, C.; Liu, L. R.; Kendrick, B. K.; Hemmerling, B.; McCarron, D. J. Hyperfine structure of the $A^1\Pi$ state of AlCl and its relevance to laser cooling and trapping. *Phys. Rev. A* **2023**, *108*, 062821.
(41) Dai, J.; Sun, Q.; Riley, B. C.; Mitra, D.; Zelevinsky, T. Laser cooling of a fermionic molecule. *Phys. Rev. Res.* **2024**, *6*, 033135.
(42) Pilgram, N. H.; Baldwin, B.; La Mantia, D. S.; Eckel, S. P.; Norrgard, E. B. Spectroscopy of laser cooling transitions in MgF. *Phys. Rev. A* **2024**, *110*, 023110.
(43) McCarron, D. Laser cooling and trapping molecules. *J. Phys. B* **2018**, *51*, 212001.
(44) Isaev, T. A. Direct laser cooling of molecules. *Phys.-Usp.* **2020**, *63*, 289.
(45) Fitch, N.; Tarbutt, M. Laser-cooled molecules. *Adv. At. Mol. Opt. Phys.* **2021**, *70*, 157.
(46) Chae, E. Laser cooling of molecules. *J. Korean Phys. Soc.* **2023**, *82*, 851.
(47) Langen, T.; Valtolina, G.; Wang, D.; Ye, J. Quantum state manipulation and cooling of ultracold molecules. *Nat. Phys.* **2024**, *20*, 702.
(48) Softley, T. P. Cold and ultracold molecules in the twenties. *Proc. R. Soc. London, Ser. A* **2023**, *479*, 20220806.
(49) Augenbraun, B. L.; Anderegg, L.; Hallas, C.; Lasner, Z. D.; Vilas, N. B.; Doyle, J. M. Direct laser cooling of polyatomic molecules. In *Advances In Atomic, Molecular, and Optical Physics*; Elsevier, 2023; Vol. *72*, pp 89−182.
(50) Isaev, T. A.; Berger, R. Polyatomic candidates for cooling of molecules with lasers from simple theoretical concepts. *Phys. Rev. Lett.* **2016**, *116*, 063006.
(51) Kozyryev, I.; Baum, L.; Matsuda, K.; Doyle, J. M. Proposal for laser cooling of complex polyatomic molecules. *ChemPhysChem* **2016**, *17*, 3641.

https://doi.org/10.1021/acs.jpca.4c06320
J. Phys. Chem. A 2025, 129, 1929−1940

(52) Ivanov, M. V.; Bangerter, F. H.; Krylov, A. I. Towards a rational design of laser-coolable molecules: Insights from equation-of-motion coupled-cluster calculations. *Phys. Chem. Chem. Phys.* **2019**, *21*, 19447.
(53) Li, M.; Kłos, J.; Petrov, A.; Kotochigova, S. Emulating optical cycling centers in polyatomic molecules. *Commun. Phys.* **2019**, *2*, 148.
(54) Zhao, C.; Yu, S.; Shin, A.; Long, X.; Atallah, T.; Caram, J.; Campbell, W. Molecules functionalized with optical cycling centers. *Bull. Am. Phys. Soc.* **2019**, *64*.
(55) Kłos, J.; Kotochigova, S. Prospects for laser cooling of polyatomic molecules with increasing complexity. *Phys. Rev. Res.* **2020**, *2*, 013384.
(56) Augenbraun, B. L.; Doyle, J. M.; Zelevinsky, T.; Kozyryev, I. Molecular asymmetry and optical cycling: laser cooling asymmetric top molecules. *Phys. Rev. X* **2020**, *10*, 031022.
(57) Zhu, G. Z.; Mitra, D.; Augenbraun, B. L.; Dickerson, C. E.; Frim, M. J.; Lao, G.; Lasner, Z. D.; Alexandrova, A. N.; Campbell, W. C.; Caram, J. R.; Doyle, J. M.; Hudson, E. R. Functionalizing aromatic compounds with optical cycling centres. *Nat. Chem.* **2022**, *14*, 995.
(58) Kozyryev, I.; Baum, L.; Matsuda, K.; Augenbraun, B. L.; Anderegg, L.; Sedlack, A. P.; Doyle, J. M. Sisyphus laser cooling of a polyatomic molecule. *Phys. Rev. Lett.* **2017**, *118*, 173201.
(59) Nguyen, D.-T.; Steimle, T. C.; Kozyryev, I.; Huang, M.; McCoy, A. B. Fluorescence branching ratios and magnetic tuning of the visible spectrum of SrOH. *J. Mol. Spectrosc.* **2018**, *347*, 7.
(60) Lasner, Z.; Lunstad, A.; Zhang, C.; Cheng, L.; Doyle, J. M. Vibronic branching ratios for nearly closed rapid photon cycling of SrOH. *Phys. Rev. A* **2022**, *106*, L020801.
(61) O'Rourke, M. J.; Hutzler, N. R. Hypermetallic polar molecules for precision measurements. *Phys. Rev. A* **2019**, *100*, 022502.
(62) Denis, M.; Haase, P. A. B.; Timmermans, R. G. E.; Eliav, E.; Hutzler, N. R.; Borschevsky, A. Enhancement factor for the electric dipole moment of the electron in the BaOH and YbOH molecules. *Phys. Rev. A* **2019**, *99*, 042512.
(63) Augenbraun, B. L.; Lasner, Z. D.; Frenett, A.; Sawaoka, H.; Miller, C.; Steimle, T. C.; Doyle, J. M. Laser-cooled polyatomic molecules for improved electron electric dipole moment searches. *New J. Phys.* **2020**, *22*, 022003.
(64) Jadbabaie, A.; Pilgram, N. H.; Kłos, J.; Kotochigova, S.; Hutzler, N. R. Enhanced molecular yield from a cryogenic buffer gas beam source via excited state chemistry. *New J. Phys.* **2020**, *22*, 022002.
(65) Mengesha, E. T.; Le, A. T.; Steimle, T. C.; Cheng, L.; Zhang, C.; Augenbraun, B. L.; Lasner, Z.; Doyle, J. Branching Ratios, Radiative Lifetimes, and Transition Dipole Moments for YbOH. *J. Phys. Chem. A* **2020**, *124*, 3135.
(66) Jadbabaie, A.; Takahashi, Y.; Pilgram, N. H.; Conn, C. J.; Zeng, Y.; Zhang, C.; Hutzler, N. R. Characterizing the fundamental bending vibration of a linear polyatomic molecule for symmetry violation searches. *New J. Phys.* **2023**, *25*, 073014.
(67) Pilgram, N. H.; Jadbabaie, A.; Conn, C. J.; Hutzler, N. R. Direct measurement of high-lying vibrational repumping transitions for molecular laser cooling. *Phys. Rev. A* **2023**, *107*, 062805.
(68) Zeng, Y.; Jadbabaie, A.; Patel, A. N.; Yu, P.; Steimle, T. C.; Hutzler, N. R. Optical cycling in polyatomic molecules with complex hyperfine structure. *Phys. Rev. A* **2023**, *108*, 012813.
(69) Mitra, D.; Vilas, N. B.; Hallas, C.; Anderegg, L.; Augenbraun, B. L.; Baum, L.; Miller, C.; Raval, S.; Doyle, J. M. Direct laser cooling of a symmetric top molecule. *Science* **2020**, *369*, 1366.
(70) Augenbraun, B. L.; Burchesky, S.; Winnicki, A.; Doyle, J. M. High-resolution laser spectroscopy of a functionalized aromatic molecule. *J. Phys. Chem. Lett.* **2022**, *13*, 10771.
(71) Isaev, T.; Oleynichenko, A. V.; Makinskii, D. A.; Zaitsevskii, A. Optical cycling in charged complexes with Ra-N bonds. *Chem. Phys. Lett.* **2024**, *845*, 141301.
(72) Isaev, T. A.; Zaitsevskii, A. V.; Eliav, E. Laser-coolable polyatomic molecules with heavy nuclei. *J. Phys. B* **2017**, *50*, 225101.
(73) Zhang, C.; Yu, P.; Conn, C. J.; Hutzler, N. R.; Cheng, L. Relativistic coupled-cluster calculations of RaOH pertinent to spectroscopic detection and laser cooling. *Phys. Chem. Chem. Phys.* **2023**, *25*, 32613.
(74) Zakharova, A., Symmetric top molecule $YbOCH_3$ in the fundamental PT-violation searches, **2024**, *854*, 141552.
(75) Yu, P.; Lopez, A.; Goddard, W. A.; Hutzler, N. R. Multivalent optical cycling centers: towards control of polyatomics with multi-electron degrees of freedom. *Phys. Chem. Chem. Phys.* **2022**, *25*, 154.
(76) Guo, H.; Dickerson, C. E.; Shin, A. J.; Zhao, C.; Atallah, T. L.; Caram, J. R.; Campbell, W. C.; Alexandrova, A. N. Surface chemical trapping of optical cycling centers. *Phys. Chem. Chem. Phys.* **2021**, *23*, 211.
(77) Dickerson, C. E.; Guo, H.; Shin, A. J.; Augenbraun, B. L.; Caram, J. R.; Campbell, W. C.; Alexandrova, A. N. Franck-Condon Tuning of Optical Cycling Centers by Organic Functionalization. *Phys. Rev. Lett.* **2021**, *126*, 123002.
(78) Dickerson, C. E.; Guo, H.; Zhu, G. Z.; Hudson, E. R.; Caram, J. R.; Campbell, W. C.; Alexandrova, A. N. Optical cycling functionalization of arenes. *J. Phys. Chem. Lett.* **2021**, *12*, 3989.
(79) Mitra, D.; Lasner, Z. D.; Zhu, G. Z.; Dickerson, C. E.; Augenbraun, B. L.; Bailey, A. D.; Alexandrova, A. N.; Campbell, W. C.; Caram, J. R.; Hudson, E. R.; Doyle, J. M. Pathway toward optical cycling and laser cooling of functionalized arenes. *J. Phys. Chem. Lett.* **2022**, *13*, 7029.
(80) Lao, G.; Zhu, G. Z.; Dickerson, C. E.; Augenbraun, B. L.; Alexandrova, A. N.; Caram, J. R.; Hudson, E. R.; Campbell, W. C. Laser spectroscopy of aromatic molecules with optical cycling centers: Strontium(I) phenoxides. *J. Phys. Chem. Lett.* **2022**, *13*, 11029.
(81) Dickerson, C. E.; Chang, C.; Guo, H.; Alexandrova, A. N. Fully saturated hydrocarbons as hosts of optical cycling centers. *J. Phys. Chem. A* **2022**, *126*, 9644.
(82) Dickerson, C. E.; Alexandrova, A. N.; Narang, P.; Philbin, J. P. Single molecule superradiance for optical cycling. *arXiv* **2023**, 2310.01534. arXiv preprint
(83) Zhu, G. Z.; Lao, G.; Dickerson, C. E.; Caram, J. R.; Campbell, W. C.; Alexandrova, A. N.; Hudson, E. R. Extending the large molecule limit: The role of Fermi resonance in developing a quantum functional group. *J. Phys. Chem. Lett.* **2024**, *15*, 590.
(84) Ivanov, M. V.; Jagau, T.-C.; Zhu, G.-Z.; Hudson, E. R.; Krylov, A. I. In search of molecular ions for optical cycling: A difficult road. *Phys. Chem. Chem. Phys.* **2020**, *22*, 17075.
(85) Wójcik, P.; Hudson, E. R.; Krylov, A. I. On the prospects of optical cycling in diatomic cations: effects of transition metals, spin−orbit couplings, and multiple bonds. *Mol. Phys.* **2022**, *121* (9−10), No. e2107582.
(86) Ivanov, M. V.; Gulania, S.; Krylov, A. I. Two cycling centers in one molecule: Communication by through-bond interactions and entanglement of the unpaired electrons. *J. Phys. Chem. Lett.* **2020**, *11*, 1297.
(87) Khvorost, T.; Wójcik, P.; Chang, C.; Calvillo, M.; Dickerson, C.; Lao, G.; Hudson, E. R.; Krylov, A. I.; Alexandrova, A. N. Dual optical cycling centers mounted on an organic scaffold: New insights from quantum chemistry calculations and symmetry analysis. *J. Phys. Chem. Lett.* **2024**, *15*, 5665−5673.
(88) Bandara, H. M. D.; Burdette, S. C. Photoisomerization in different classes of azobenzene. *Chem. Soc. Rev.* **2012**, *41*, 1809−1825.
(89) Beharry, A. A.; Woolley, G. A. Azobenzene photoswitches for biomolecules. *Chem. Soc. Rev.* **2011**, *40*, 4422.
(90) Kojima, M.; Nebashi, S.; Ogawa, K.; Kurita, N. Effect of solvent on cis-to-trans isomerization of 4-hydroxyazobenzene aggregated through intermolecular hydrogen bonds. *J. Phys. Org. Chem.* **2005**, *18*, 994.
(91) Poutanen, M.; Ahmed, Z.; Rautkari, L.; Ikkala, O.; Priimagi, A. Thermal isomerization of hydroxyazobenzenes as a platform for vapor sensing. *ACS Macro Lett.* **2018**, *7*, 381.
(92) Krylov, A. I. The quantum chemistry of open-shell species. In *Reviews in Computational Chemistry*; Parrill, A. L., Lipkowitz, K. B., Eds.; Wiley & Sons, 2017; Vol. *30*, pp 151−224.
(93) Krylov, A. I. Equation-of-motion coupled-cluster methods for open-shell and electronically excited species: The hitchhiker's guide to Fock space. *Annu. Rev. Phys. Chem.* **2008**, *59*, 433.

https://doi.org/10.1021/acs.jpca.4c06320
J. Phys. Chem. A 2025, 129, 1929−1940

(94) Sneskov, K.; Christiansen, O. Excited state coupled cluster methods. *Wiley Interdiscip. Rev.:Comput. Mol. Sci.* **2012**, *2*, 566.
(95) Bartlett, R. J. Coupled-cluster theory and its equation-of-motion extensions. *Wiley Interdiscip. Rev.:Comput. Mol. Sci.* **2012**, *2*, 126.
(96) Gulania, S.; Kjønstad, E. F.; Stanton, J. F.; Koch, H.; Krylov, A. I. Equation-of-motion coupled-cluster method with double electron-attaching operators: Theory, implementation, and benchmarks. *J. Chem. Phys.* **2021**, *154*, 114115.
(97) Levchenko, S. V.; Krylov, A. I. Equation-of-motion spin-flip coupled-cluster model with single and double substitutions: Theory and application to cyclobutadiene. *J. Chem. Phys.* **2004**, *120*, 175.
(98) Bartlett, R. J.; Musiał, M. Coupled-cluster theory in quantum mechanics. *Rev. Mod. Phys.* **2007**, *79*, 291.
(99) Simons, J.; Smith, W. D. Theory of electron affinities of small molecules. *J. Chem. Phys.* **1973**, *58*, 4899.
(100) Nooijen, M.; Bartlett, R. J. Equation of motion coupled cluster method for electron attachment. *J. Chem. Phys.* **1995**, *102*, 3629.
(101) Simons, J. Equation of motion (EOM) methods for computing electron affinities. In *Encyclopedia of computational chemistry*; Wiley & Son: New York, 1998; .
(102) Stanton, J. F.; Bartlett, R. J. The equation of motion coupled-cluster method. A systematic biorthogonal approach to molecular excitation energies, transition probabilities, and excited state properties. *J. Chem. Phys.* **1993**, *98*, 7029.
(103) Stanton, J. F.; Gauss, J. A discussion on some problems associated with the quantum mechanical treatment of open-shell molecules. *Adv. Chem. Phys.* **2003**, *125*, 101.
(104) Reisler, H.; Krylov, A. I. Interacting Rydberg and valence states in radicals and molecules: Experimental and theoretical studies. *Int. Rev. Phys. Chem.* **2009**, *28*, 267.
(105) Krylov, A. I. Size-consistent wave functions for bond-breaking: The equation-of-motion spin-flip model. *Chem. Phys. Lett.* **2001**, *338*, 375.
(106) Levchenko, S. V.; Wang, T.; Krylov, A. I. Analytic gradients for the spin-conserving and spin-flipping equation-of-motion coupled-cluster models with single and double substitutions. *J. Chem. Phys.* **2005**, *122*, 224106.
(107) Krylov, A. I. The spin-flip equation-of-motion coupled-cluster electronic structure method for a description of excited states, bond-breaking, diradicals, and triradicals. *Acc. Chem. Res.* **2006**, *39*, 83.
(108) Casanova, D.; Krylov, A. I. Spin-flip methods in quantum chemistry. *Phys. Chem. Chem. Phys.* **2020**, *22*, 4326.
(109) Musiał, M.; Kucharski, S. A.; Bartlett, R. J. Multireference double electron attached coupled cluster method with full inclusion of the connected triple excitations: MR-DA-CCSDT. *J. Chem. Theory Comput.* **2011**, *7*, 3088−3096.
(110) Perera, A.; Molt, R. W.; Lotrich, V. F.; Bartlett, R. J. Singlet-triplet separations of di-radicals treated by the DEA/DIP-EOM-CCSD methods. In *Isaiah. Shavitt: A memorial festschrift from theoretical chemistry accounts*; Cramer, C. J., Truhlar, D. G., Eds.; Springer, 2016; Vol. *9*, pp 153−165.
(111) Dunning, T. H., Jr. Gaussian basis sets for use in correlated molecular calculations. I. The atoms boron through neon and hydrogen. *J. Chem. Phys.* **1989**, *90*, 1007.
(112) Koput, J.; Peterson, K. A. Ab initio potential energy surface and vibrational−rotational energy levels of $X^2\Sigma^+$ CaOH. *J. Phys. Chem. A* **2002**, *106*, 9595.
(113) Kendall, R. A.; Dunning, T. H., Jr.; Harrison, R. J. Electron affinities of the first-row atoms revisited. Systematic basis sets and wavefunctions. *J. Chem. Phys.* **1992**, *96*, 6796.
(114) Epifanovsky, E.; Gilbert, A. T. B.; Feng, X.; Lee, J.; Mao, Y.; Mardirossian, N.; Pokhilko, P.; White, A. F.; Coons, M. P.; Dempwolff, A. L.; et al. Software for the frontiers of quantum chemistry: An overview of developments in the Q-Chem 5 package. *J. Chem. Phys.* **2021**, *155*, 084801.
(115) Krylov, A. I.; Gill, P. M. W. Q-Chem: An engine for innovation. *Wiley Interdiscip. Rev.:Comput. Mol. Sci.* **2013**, *3*, 317.
(116) Gilbert, A. T. B. *IQmol molecular viewer*, 2024. http://iqmol.org (accessed 12/7/2024).
(117) Jmol development team. *Jmol: an open-source Java viewer for chemical structures in 3D*, 2024. http://www.jmol.org/ (accessed 12/7/2024).
(118) Krylov, A. I. From orbitals to observables and back. *J. Chem. Phys.* **2020**, *153*, 080901.
(119) Mewes, S. A.; Plasser, F.; Krylov, A.; Dreuw, A. Benchmarking excited-state calculations using exciton properties. *J. Chem. Theory Comput.* **2018**, *14*, 710.
(120) Bäppler, S. A.; Plasser, F.; Wormit, M.; Dreuw, A. Exciton analysis of many-body wave functions: Bridging the gap between the quasiparticle and molecular orbital pictures. *Phys. Rev. A* **2014**, *90*, 052521.
(121) Plasser, F.; Wormit, M.; Dreuw, A. New tools for the systematic analysis and visualization of electronic excitations. I. Formalism. *J. Chem. Phys.* **2014**, *141*, 024106.
(122) Plasser, F. Theodore: a toolbox for a detailed and automated analysis of electronic excited state computations. *J. Chem. Phys.* **2020**, *152*, 084108.
(123) Bernath, P. F.; Brazier, C. R. Spectroscopy of CaOH. *Astrophys. J.* **1985**, *288*, 373.
(124) Steimle, T. C.; Fletcher, D. A.; Jung, K. Y.; Scurlock, C. T. A supersonic molecular beam optical Stark study of CaOH and SrOH. *J. Chem. Phys.* **1992**, *96*, 2556.
(125) Scurlock, C.; Fletcher, D.; Steimle, T. Hyperfine structure in the (0,0,0) $X^2\Sigma^+$ state of CaOH observed by pump/probe microwave-optical double resonance. *J. Mol. Spectrosc.* **1993**, *159*, 350.
(126) Hilborn, R. C.; Qingshi, Z.; Harris, D. O. Laser spectroscopy of the A-X transitions of CaOH and CaOD. *J. Mol. Spectrosc.* **1983**, *97*, 73.
(127) Bernath, P.; Kinsey-Nielsen, S. Dye laser spectroscopy of the $B^2\Sigma^+$-$X^2\Sigma^+$ transition of CaOH. *Chem. Phys. Lett.* **1984**, *105*, 663.
(128) Miyamoto, Y.; Tobaru, R.; Takahashi, Y.; Hiramoto, A.; Iwakuni, K.; Kuma, S.; Enomoto, K.; Baba, M. Doppler-free spectroscopy of buffer-gas-cooled calcium monohydroxide. *J. Phys. Chem. A* **2023**, *127*, 4758.
(129) Taylor, C. M.; Chaudhuri, R. K.; Freed, K. F. Electronic structure of the calcium monohydroxide radical. *J. Chem. Phys.* **2005**, *122*, 044317.
(130) Koput, J.; Peterson, K. A. *Ab Initio* Potential energy surface and vibrational-rotational energy levels of $X^2\Sigma^+$ CaOH. *J. Phys. Chem. A* **2002**, *106*, 9595.
(131) Kozyryev, I.; Steimle, T. C.; Yu, P.; Nguyen, D.-T.; Doyle, J. M. Determination of CaOH and $CaOCH_3$ vibrational branching ratios for direct laser cooling and trapping. *New J. Phys.* **2019**, *21*, 052002.
(132) Baum, L.; Vilas, N. B.; Hallas, C.; Augenbraun, B. L.; Raval, S.; Mitra, D.; Doyle, J. M. 1D magneto-optical trap of polyatomic molecules. *Phys. Rev. Lett.* **2020**, *124*, 133201.
(133) Vilas, N. B.; Hallas, C.; Anderegg, L.; Robichaud, P.; Winnicki, A.; Mitra, D.; Doyle, J. M. Magneto-optical trapping and sub-Doppler cooling of a polyatomic molecule. *Nature* **2022**, *606*, 70.
(134) Baum, L.; Vilas, N. B.; Hallas, C.; Augenbraun, B. L.; Raval, S.; Mitra, D.; Doyle, J. M. Establishing a nearly closed cycling transition in a polyatomic molecule. *Phys. Rev. A* **2021**, *103*, 043111.
(135) Vilas, N. B.; Robichaud, P.; Hallas, C.; Li, G. K.; Anderegg, L.; Doyle, J. M. An optical tweezer array of ultracold polyatomic molecules. *Nature* **2024**, *628*, 282.
(136) Hallas, C.; Vilas, N. B.; Anderegg, L.; Robichaud, P.; Winnicki, A.; Zhang, C.; Cheng, L.; Doyle, J. M. Optical trapping of a polyatomic molecule in an l-type parity doublet state. *Phys. Rev. Lett.* **2023**, *130*, 153202.
(137) Anderegg, L.; Vilas, N. B.; Hallas, C.; Robichaud, P.; Jadbabaie, A.; Doyle, J. M.; Hutzler, N. R. Quantum control of trapped polyatomic molecules for eedm searches. *Science* **2023**, *382*, 665.
(138) Paul, A. C.; Sharma, K.; Telfah, H.; Miller, T. A.; Liu, J. Electronic spectroscopy of the $\tilde{A}_1^2$ A″/$\tilde{A}_2^2$ A′−$\tilde{X}^2$A′ transitions of jet-cooled calcium ethoxide radicals: Vibronic structure of alkaline earth monoalkoxide radicals of C_s symmetry. *J. Chem. Phys.* **2021**, *155*, 024301.
(139) Szalay, P. G.; Gauss, J. Spin-restricted open-shell coupled-cluster theory for excited states. *J. Chem. Phys.* **2000**, *112*, 4027.

https://doi.org/10.1021/acs.jpca.4c06320
J. Phys. Chem. A 2025, 129, 1929−1940

(140) Nguyen, T. L.; Saleh, M. A. Thermal degradation of azobenzene dyes. *Results Chem.* **2020**, *2*, 100085.
(141) Jerca, F. A.; Jerca, V. V.; Hoogenboom, R. Advances and opportunities in the exciting world of azobenzenes. *Nat. Rev. Chem* **2022**, *6*, 51.
(142) Merino, E. Synthesis of azobenzenes: the coloured pieces of molecular materials. *Chem. Soc. Rev.* **2011**, *40*, 3835.

https://doi.org/10.1021/acs.jpca.4c06320
J. Phys. Chem. A 2025, 129, 1929−1940